Generalized Perfectly Matched Layer for the Absorption of Propagating and Evanescent Waves in Lossless and Lossy Media

Jiayuan Fang, *Member, IEEE,* and Zhonghua Wu, *Student Member, IEEE*

Abstract— **The perfectly matched layer (PML), proposed by Berenger, has been proved very effective in absorbing propagating waves in lossless media. However, it has been found that the original construction of PML cannot effectively absorb evanescent waves. Also, significant reflection can appear as PML is applied to terminate lossy media. This paper describes a generalized perfectly matched layer (GPML) that extends the original PML to absorb both propagating and evanescent waves in lossless and lossy media. The generalized perfectly matched layer is derived from the Maxwell s equations in stretched coordinates and can be easily implemented in finite-difference time-domain (FDTD) programs. This paper also presents proper selection of parameters in the numerical implementation of the generalized perfectly matched layer to achieve good performance in absorption.**

I. Introduction

THE PERFECTLY matched layer (PML), recently proposed by Berenger, is an artificial lossy material used as an absorber for truncating numerical computation domains in finite-difference time-domain (FDTD) computations [1]. With this technique, certain field components are split into subcomponents and additional material parameters are introduced so that the impedance of the PML is matched to that of the free-space or internal lossless media at all frequencies and all incident angles. In contrast, previously developed lossy absorbers can typically match the interior media at only the normal incident angle [2]. It has been verified in many applications that the perfectly matched layer can absorb outgoing waves much more effectively than previously developed absorbers and many local absorbing boundary conditions [1], [3].

Recent studies have found that although the perfectly matched layer is very effective in absorbing propagating waves in lossless media, PML is not effective in absorbing evanescent waves [4]–[7]. Moreover, the original PML absorbers are only applicable to interior lossless media. For terminating lossy materials, PML can only match a special type of lossy material when its electric and magnetic conductivities satisfy a particular relation. In general, significant reflections will appear at the interface of PML and an interior lossy medium. Therefore, the original form of the PML is not a good choice for applications involving modeling wave propagation in lossy media.

A modification of the original PML has been proposed in [5] for the absorption of evanescent waves where interior media are lossless. The modification of PML for frequency domain finite-element applications presented in [8] made PML applicable to lossy media as well. In this paper, a type of absorber that can effectively absorb propagating and evanescent waves for both interior lossless and lossy media is presented for FDTD applications. We call this absorber the generalized perfectly matched layer (GPML) which, under special circumstances, becomes the original PML. Following the recently published letter on the introduction of the GPML [9], this paper presents a more detailed derivation and more numerical examples to demonstrate the performance of GPML. Proper numerical implementation of GPML will also be discussed in detail in following sections.

II. Performance of PML for Absorbing Evanescent Waves and in Lossy Media

Consider the configuration shown in Fig. 1, where the interior lossless medium is in the region $z<0$, and the perfectly matched layer with $\sigma_x = \sigma_y = 0$ is in the region $z>0$. Assume a plane wave propagates in the direction parallel to the x-z plane and of an angle θ with the z axis. Let ψ be any field component of the plane wave, then from [1, eq. 15], as the plane wave enters the PML, the field component in PML can be expressed as

$$\psi = \psi_0 e^{j\omega(t-[z\cos\theta - x\sin\theta]/c)} e^{-(\sigma_z \cos\theta/\epsilon c)z} \tag{1}$$

where σ_z is the electric conductivity of the PML medium. The last exponential of (1) rules the magnitude of the wave in PML. For a propagating wave in the z direction, $\cos\theta$ is a real number and the term $e^{-\sigma_z \cos\theta/(\epsilon c)z}$ determines that the wave decreases exponentially in the z direction. On the other hand, if the variation of the field in the z direction is of evanescent nature, $\cos\theta$ will be an imaginary number, the term $e^{-\sigma_z \cos\theta/(\epsilon c)z}$ no longer decays in the z direction and the PML does not add any additional attenuation to the wave. Therefore, in regions where fields are evanescent in the direction normal to PML/interior-medium interfaces, PML absorbers cannot provide any help in reducing the reflection.

Manuscript received December 12, 1995; revised August 26, 1996. This work is supported in part by the National Science Foundation under contract MIP-9357561 and the Integrated Electronics Engineering Research Center (IEEC) at the State University of New York at Binghamton.

The authors are with the Department of the Department of Electrical Engineering, State University of New York at Binghamton, Binghamton, NY 13902 USA.

Publisher Item Identifier S 0018-9480(96)08512-2.

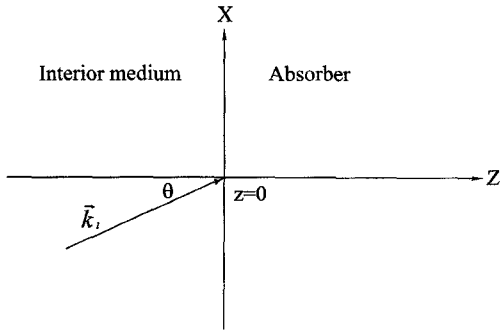

Fig. 1. Configuration of an interior lossless medium terminated with a PML absorber. A plane wave propagates in the direction parallel to the x-z plane and of an angle θ with the z axis.

Serious problems arise when PML is used to terminate interior lossy media. In the above example of a lossless interior medium, the conductivities of the PML are chosen as $\sigma_x = \sigma_y = 0$, and

$$\sigma_z/\epsilon = \sigma_z^*/\mu \tag{2}$$

so that the impedance of the PML, as proved by Berenger [1], is the same as that of the interior lossless medium for any incident angles. If the interior medium is lossy, say with a constant electric conductivity σ_0, then the PML specified by (2) and either $\sigma_x = \sigma_y = 0$ or $\sigma_x = \sigma_y = \sigma_x^*\epsilon/\mu = \sigma_y^*\epsilon/\mu = \sigma_0$ no longer matches the interior medium even at the normal incident angle. At the normal incidence, for example, the impedance of the PML is $\sqrt{\mu/\epsilon}$, whereas the impedance of the interior lossy medium is $\sqrt{\mu/(\epsilon + \sigma_0/j\omega)}$. Therefore, significant reflections can be expected from the interface of the PML and the interior lossy medium. This limitation of PML excludes the application of PML to many problems that involve lossy media.

III. Derivation of Generalized Perfectly Matched Layer

The formulation of the generalized perfectly matched layer is to be derived with the modified Maxwell's equations in the stretched coordinates. The modified Maxwell's equations in the stretched coordinates have been used in [10] to re-derive the original PML proposed by Berenger and in [5] to derive the modified PML for absorbing evanescent waves. Similar notations and procedures are used in the following derivations as those in [5] and [10].

Consider a medium with isotropic parameters $(\epsilon, \mu, \sigma_0, \sigma_0^*)$, where σ_0 and σ_0^* are not necessarily related by (2), the frequency domain modified Maxwell's equations in the stretched coordinates can be written as

$$\nabla_s \times \vec{E} = -j\omega\mu'\vec{H} \tag{3}$$

$$\nabla_s \times \vec{H} = j\omega\epsilon'\vec{E} \tag{4}$$

where $\mu' = \mu + \sigma_0^*/j\omega, \epsilon' = \epsilon + \sigma_0/j\omega$, and

$$\nabla_s = \vec{a}_x\frac{1}{s_x}\frac{\partial}{\partial x} + \vec{a}_y\frac{1}{s_y}\frac{\partial}{\partial y} + \vec{a}_z\frac{1}{s_z}\frac{\partial}{\partial z}. \tag{5}$$

s_x, s_y, and s_z are the coordinate stretching variables in the x, y, and z directions.

Substitute a general plane-wave solution

$$\vec{E} = \vec{E}_0 e^{-j\vec{k}\cdot\vec{r}} \tag{6}$$

$$\vec{H} = \vec{H}_0 e^{-j\vec{k}\cdot\vec{r}} \tag{7}$$

where $\vec{k} = \vec{a}_x k_x + \vec{a}_y k_y + \vec{a}_z k_z$, into (3) and (4) gives

$$\vec{k}_s \times \vec{E} = \omega\mu'\vec{H} \tag{8}$$

$$\vec{k}_s \times \vec{H} = -\omega\epsilon'\vec{E} \tag{9}$$

where

$$\vec{k}_s = \vec{a}_x\frac{k_x}{s_x} + \vec{a}_y\frac{k_y}{s_y} + \vec{a}_z\frac{k_z}{s_z}. \tag{10}$$

Combining (8) and (9)

$$\begin{aligned} -\omega^2\mu'\epsilon'\vec{E} &= \vec{k}_s \times \vec{k}_s \times \vec{E} \\ &= \vec{k}_s(\vec{k}_s \cdot \vec{E}) - k_s^2\vec{E}. \end{aligned} \tag{11}$$

From (9), $\vec{k}_s \cdot \vec{E} = 0$, then from (10) and (11), we have

$$k^2 = \omega^2\mu'\epsilon' = k_s^2 = \frac{k_x^2}{s_x^2} + \frac{k_y^2}{s_y^2} + \frac{k_z^2}{s_z^2}. \tag{12}$$

Assume that two media with parameters (ϵ_1', μ_1') and (ϵ_2', μ_2') are interfaced at $z = 0$, and a plane wave of arbitrary polarization is obliquely incident on the interface from medium 1. Suppose the incident plane-wave propagates in the direction of angles θ and ϕ to the z and x axes, then

$$k_x = ks_x \sin\theta\cos\phi \tag{13}$$

$$k_y = ks_y \sin\theta\sin\phi \tag{14}$$

$$k_z = ks_z \cos\theta. \tag{15}$$

The incident field can be decomposed into a sum of two components, one with the electric field perpendicular to the plane of incident and the other with the electric field parallel to the plane of incident. Applying the continuity conditions for the tangential electric and magnetic fields at the interface, the reflection coefficients of these two components can be derived straightforwardly in the same way as that in [10]

$$R_\perp = \frac{k_1\cos\theta_1\mu_2' - k_2\cos\theta_2\mu_1'}{k_1\cos\theta_1\mu_2' + k_2\cos\theta_2\mu_1'} \tag{16}$$

$$R_{||} = \frac{k_1\cos\theta_1\epsilon_2' - k_2\cos\theta_2\epsilon_1'}{k_1\cos\theta_1\epsilon_2' + k_2\cos\theta_2\epsilon_1'}. \tag{17}$$

The phase matching condition at the interface requires that $k_{1x} = k_{2x}$ and $k_{1y} = k_{2y}$, i.e.,

$$k_1 s_{1x}\sin\theta_1\cos\phi_1 = k_2 s_{2x}\sin\theta_2\cos\theta_2 \tag{18}$$

and

$$k_1 s_{1y}\sin\theta_1\sin\phi_1 = k_2 s_{2y}\sin\theta_2\sin\phi_2. \tag{19}$$

If we choose

$$\begin{aligned} \epsilon_1' &= \epsilon_2' \\ \mu_1' &= \mu_2' \\ s_{1x} &= s_{2x} \\ s_{1y} &= s_{2y} \end{aligned} \tag{20}$$

then from (12), $k_1 = k_2$, and from (18) and (19), $\theta_1 = \theta_2$ and $\phi_1 = \phi_2$. Subsequently, the two media, which can have arbitrary electric loss (σ_0) and arbitrary magnetic loss (σ_0^*), are perfectly matched because from (16) and (17), $R_\perp = R_{||} = 0$ for all angles of incidence and all frequencies.

Assume medium 1 is the interior region and medium 2 is a perfectly matched absorber, then in medium 1, which is a real physical medium, $(s_{1x}, s_{1y}, s_{1z}) = (1, 1, 1)$; and in medium 2, which is an artificial absorbing medium, the stretching coordinate variables should be chosen as $(s_{2x}, s_{2y}, s_{2z}) = (1, 1, s_z)$ to guarantee no reflection at the interface. The term s_z is in general a complex number and can be chosen in the following form:

$$s_z(z) = s_{z0}(z)\left[1 + \frac{\sigma_z(z)}{j\omega\epsilon}\right]. \tag{21}$$

The terms $s_{z0}(z)$ and $\sigma_z(z)$ are functions of z and need to be selected carefully to avoid numerical reflections in the absorber. Proper selection of $s_{z0}(z)$ and $\sigma_z(z)$ will be discussed in Section V.

The plane wave solution in the GPML absorber can then be derived as

$$\begin{aligned}\psi &= \psi_0 e^{j(\omega t - \vec{k}\cdot\vec{r})} \\ &= \psi_0 e^{j(\omega t - jk\sin\theta x)} e^{-jks_z\cos\theta z}.\end{aligned} \tag{22}$$

In the last exponential of (22), if let $k\cos\theta = k_z' - jk_z''$, then

$$\begin{aligned}\psi = \psi_0 e^{j(\omega t - k\sin\theta x)} &\exp\left[-j\left(k_z' - \frac{k_z''\sigma_z}{\omega\epsilon}\right)s_{z0}(z)z\right] \\ &\cdot \exp\left[-\left(k_z'' + \frac{k_z'\sigma_z}{\omega\epsilon}\right)s_{z0}(z)z\right].\end{aligned} \tag{23}$$

If the plane wave is mainly a propagating wave, i.e., k_z' is dominant, the amplitude of the wave decays mainly as $e^{-(k_z'\sigma_z/\omega\epsilon)s_{z0}(z)z}$, which is similar to the behavior of the wave in the original PML. If the plane wave is evanescent in the z direction, i.e., k_z'' is dominant, the wave decays mainly as $e^{-k_z''s_{z0}(z)z}$, whereas in the original PML, the evanescent wave decays as $e^{-k_z''z}$. By choosing $s_{z0}(z) > 1$, the attenuation of the evanescent wave is accelerated. A potential problem that can be noticed from (23) is that if k_z' is negative, which may happen for evanescent waves when medium is lossy, the last exponential in (23) may increase rather than decrease with z at low frequencies.

From (3), (4), and (21), and with the notation of subcomponents proposed by Berenger [1], the frequency domain equations for the field components in the generalized perfectly matched layer can then be written as

$$-\frac{\partial H_x}{s_{y0}(y)\partial y} = \left(j\omega\epsilon + \sigma_0 + \sigma_y + \frac{\sigma_0\sigma_y}{j\omega\epsilon}\right)E_{zy} \tag{24}$$

$$\frac{\partial H_x}{s_{z0}(z)\partial z} = \left(j\omega\epsilon + \sigma_0 + \sigma_z + \frac{\sigma_0\sigma_z}{j\omega\epsilon}\right)E_{yz} \tag{25}$$

$$-\frac{\partial H_y}{s_{z0}(z)\partial z} = \left(j\omega\epsilon + \sigma_0 + \sigma_z + \frac{\sigma_0\sigma_z}{j\omega\epsilon}\right)E_{xz} \tag{26}$$

$$\frac{\partial H_y}{s_{x0}(x)\partial x} = \left(j\omega\epsilon + \sigma_0 + \sigma_x + \frac{\sigma_0\sigma_x}{j\omega\epsilon}\right)E_{zx} \tag{27}$$

$$-\frac{\partial H_z}{s_{x0}(x)\partial x} = \left(j\omega\epsilon + \sigma_0 + \sigma_x + \frac{\sigma_0\sigma_x}{j\omega\epsilon}\right)E_{yx} \tag{28}$$

$$\frac{\partial H_z}{s_{y0}(y)\partial y} = \left(j\omega\epsilon + \sigma_0 + \sigma_y + \frac{\sigma_0\sigma_y}{j\omega\epsilon}\right)E_{xy} \tag{29}$$

$$\frac{\partial E_x}{s_{y0}(y)\partial y} = \left(j\omega\mu + \sigma_0^* + \sigma_y^* + \frac{\sigma_0^*\sigma_y^*}{j\omega\mu}\right)H_{zy} \tag{30}$$

$$-\frac{\partial E_x}{s_{z0}(z)\partial x} = \left(j\omega\mu + \sigma_0^* + \sigma_z^* + \frac{\sigma_0^*\sigma_z^*}{j\omega\mu}\right)H_{yz} \tag{31}$$

$$\frac{\partial E_y}{s_{z0}(z)\partial z} = \left(j\omega\mu + \sigma_0^* + \sigma_z^* + \frac{\sigma_0^*\sigma_z^*}{j\omega\mu}\right)H_{xz} \tag{32}$$

$$-\frac{\partial E_y}{s_{x0}(x)\partial x} = \left(j\omega\mu + \sigma_0^* + \sigma_x^* + \frac{\sigma_0^*\sigma_x^*}{j\omega\mu}\right)H_{zx} \tag{33}$$

$$\frac{\partial E_z}{s_{x0}(x)\partial x} = \left(j\omega\mu + \sigma_0^* + \sigma_x^* + \frac{\sigma_0^*\sigma_x^*}{j\omega\mu}\right)H_{yx} \tag{34}$$

$$-\frac{\partial E_z}{s_{y0}(y)\partial y} = \left(j\omega\mu + \sigma_0^* + \sigma_y^* + \frac{\sigma_0^*\sigma_y^*}{j\omega\mu}\right)H_{xy} \tag{35}$$

where $\sigma_x/\epsilon = \sigma_x^*/\mu, \sigma_y/\epsilon = \sigma_y^*/\mu$ and $\sigma_z/\epsilon = \sigma_z^*/\mu$, but σ_0 and σ_0^* may not satisfy $\sigma_0/\epsilon = \sigma_0^*/\mu$. It can be shown that if $\sigma_0 = \sigma_0^* = 0$ and $s_{x0}(x) = s_{y0}(y) = s_{z0}(z) = 1$, then (24) to (35) return to the original formulation of Berenger's PML [1], [3].

IV. Finite-Difference Implementation of GPML

The time-domain equations corresponding to GPML can be converted from the frequency-domain equations (24)–(35). For the convenience of illustration, let's consider the two-dimensional (2-D) TE^z case with $E_z = 0$ and $\partial/\partial z = 0$. We have

$$\frac{\partial E_x}{s_{y0}(y)\partial y} = \left(j\omega\mu + \sigma_0^* + \sigma_y^* + \frac{\sigma_0^*\sigma_y^*}{j\omega\mu}\right)H_{zy} \tag{36}$$

$$-\frac{\partial E_y}{s_{x0}(x)\partial x} = \left(j\omega\mu + \sigma_0^* + \sigma_x^* + \frac{\sigma_0^*\sigma_x^*}{j\omega\mu}\right)H_{zx} \tag{37}$$

$$-\frac{\partial H_z}{s_{x0}(x)\partial x} = \left(j\omega\epsilon + \sigma_0 + \sigma_x + \frac{\sigma_0\sigma_x}{j\omega\epsilon}\right)E_y \tag{38}$$

$$\frac{\partial H_z}{s_{y0}(y)\partial y} = \left(j\omega\epsilon + \sigma_0 + \sigma_y + \frac{\sigma_0\sigma_y}{j\omega\epsilon}\right)E_x. \tag{39}$$

Introducing auxiliary variables

$$E_x^I = \frac{1}{j\omega}E_x \tag{40}$$

$$E_y^I = \frac{1}{j\omega}E_y \tag{41}$$

$$H_{zx}^I = \frac{1}{j\omega}H_{zx} \tag{42}$$

$$H_{zy}^I = \frac{1}{j\omega}H_{zy} \tag{43}$$

which are the time integration of corresponding field components. Transferring (36) to (43) into the time-domain, we get

$$\frac{\partial E_y}{s_{y0}(y)\partial y} = \mu\frac{\partial H_{zy}}{\partial t} + (\sigma_0^* + \sigma_y^*)H_{zy} + \frac{\sigma_0^*\sigma_y^*}{\mu}H_{zy}^I \tag{44}$$

$$-\frac{\partial E_y}{s_{x0}(x)\partial x} = \mu\frac{\partial H_{zx}}{\partial t} + (\sigma_0^* + \sigma_x^*)H_{zx} + \frac{\sigma_0^*\sigma_x^*}{\mu}H_{zx}^I \tag{45}$$

$$-\frac{\partial H_z}{s_{x0}(x)\partial x} = \epsilon\frac{\partial E_y}{\partial t} + (\sigma_0 + \sigma_x)E_y + \frac{\sigma_0\sigma_x}{\epsilon}E_y^I \tag{46}$$

$$\frac{\partial H_z}{s_{y0}(y)\partial y} = \epsilon\frac{\partial E_x}{\partial t} + (\sigma_0 + \sigma_y)E_x + \frac{\sigma_0\sigma_y}{\epsilon}E_x^I \tag{47}$$

and

$$\frac{\partial E_x^I}{\partial t} = E_x \tag{48}$$

$$\frac{\partial E_y^I}{\partial t} = E_y \tag{49}$$

$$\frac{\partial H_{zx}^I}{\partial t} = H_{zx} \tag{50}$$

$$\frac{\partial H_{zy}^I}{\partial t} = H_{zy}. \tag{51}$$

The discretization of (44)–(51) follows the standard central difference approach. For example, the difference equation of (45) is

$$\begin{aligned} H_{zx}^{n+1/2}&(i+1/2, j+1/2) \\ &= \frac{\mu/\Delta t - (\sigma_0^* + \sigma_x^*)/2}{\mu/\Delta t + (\sigma_0^* + \sigma_x^*)/2} H_{zx}^{n-1/2}(i+1/2, j+1/2) \\ &\quad - \frac{1}{(\mu/\Delta t + (\sigma_0^* + \sigma_x^*)/2)s_{x0}(x)\Delta x} \\ &\quad \cdot [E_y^n(i+1, j+1/2) - E_y^n(i, j+1/2)] \\ &\quad - \frac{\sigma_0^*\sigma_x^*}{\mu}\frac{1}{\mu/\Delta t + (\sigma_0^* + \sigma_x^*)/2} H_{zx}^{In}(i+1/2, j+1/2). \end{aligned} \tag{52}$$

The term $H_{zx}^{In}(i+1/2, j+1/2)$ in (52) can be found through discretizing (50) as

$$\begin{aligned} H_{zx}^{In}(i+1/2, j+1/2) &= H_{zx}^{In-1}(i+1/2, j+1/2) \\ &\quad + \Delta t H_{zx}^{n-1/2}(i+1/2, j+1/2). \end{aligned} \tag{53}$$

For TM^z fields and general 3-D fields, the corresponding finite difference equations can be derived in the same way as above.

V. Selection of Material Parameters

The parameters $s_{x0}(x), s_{y0}(y), s_{z0}(z), \sigma_x(x), \sigma_y(y)$ and $\sigma_z(z)$ need to be properly chosen to have the absorber perform effectively. Theoretically, the larger the values of these parameters, the faster the attenuation of fields in the absorber. However, if the parameters $s_{x0}(x), s_{y0}(y), s_{z0}(z), \sigma_x(x), \sigma_y(y)$ and $\sigma_z(z)$ vary with space, numerical discretization errors associated with the finite-difference equations make the absorber approximately, instead of perfectly, match the interior media and cause certain reflection as a wave travels through the absorber. The steeper the variation of these parameters, the larger the numerical reflection. Therefore, to avoid significant numerical reflections, these parameters have to be increased gradually and continuously to their largest values.

In the formulation of PML presented by Berenger [1], the conductivity profile in PML is chosen as, take $\sigma_z(z)$ as an example

$$\sigma_z(z) = \sigma_m\left(\frac{z}{\delta}\right)^n \tag{54}$$

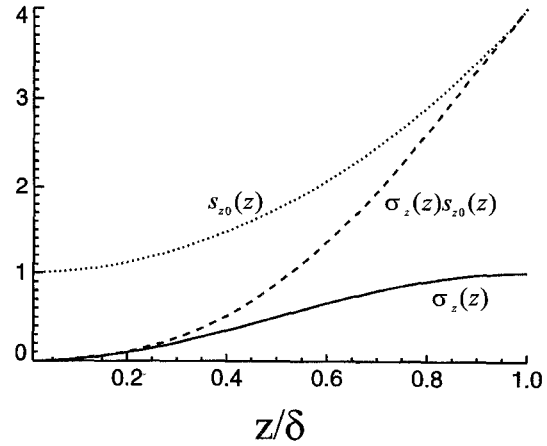

Fig. 2. Curves of $s_{z0}(z), \sigma_z(z)$ and $s_{z0}(z)\sigma_z(z)$ vs. the ratio z/δ when $n = 2, s_m = 3$ in (55) and $\sigma_m = 1$ in (56).

where δ is the thickness of the absorber and z is the distance to the interface of the PML and the internal medium. Optimum values of σ_m and n depend on the thickness of the absorber δ. The thicker the absorber, the larger the optimum values of σ_m and n are. Some numerical experiments of the selection of σ_m and n for various absorber thicknesses are presented in [6] and [11]–[13].

For the generalized perfectly matched layer presented in the last section, patterns of both $s_{z0}(z)$ and $\sigma_z(z)$ need to be determined. From (23), it can be found that for propagating waves, the fields attenuate according to $e^{-(s_{z0}(z)\sigma_z(z)/\omega\epsilon)k_z z}$; and for evanescent waves, the fields attenuate in the rate of $e^{-s_{z0}(z)|k_z|z}$, provided that $k_z'\sigma_z/\omega\epsilon$ is negligible compared with k_z'' in the frequency range of interest. Our objective is to properly select $s_{z0}(z)$ and $\sigma_z(z)$ so that the absorber can effectively absorb both propagating and evanescent waves. First, we let the product of $s_{z0}(z)$ and $\sigma_z(z)$ change gradually with space, and we select

$$s_{z0}(z) = 1 + s_m\left(\frac{z}{\delta}\right)^n \tag{55}$$

$$\sigma_z(z) = \sigma_m \sin^2\left(\frac{\pi z}{2\delta}\right). \tag{56}$$

When $s_{z0}(z)$ and $\sigma_z(z)$ are chosen as (55) and (56), the product of $s_{z0}(z)$ and $\sigma_z(z)$ changes with space nearly in z^2 as z closes to zero, and approximately in z^n as z closes to δ. Numerical tests show that, for propagating waves, the effect of the absorber with $s_{z0}(z)$ and $\sigma_z(z)$ chosen as (55) and (56) is about the same as that of the original PML with $\sigma_z(z)$ chosen as (54). If $s_{z0}(z)$ is chosen as (55) and $\sigma_z(z)$ is chosen as (54) instead of (56), then the product of $s_{z0}(z)$ and $\sigma_z(z)$ can vary too fast as z closes to δ, and consequently large numerical reflection may appear. Fig. 2 shows patterns of $s_{z0}(z), \sigma_z(z)$ and $s_{z0}(z)\sigma_z(z)$, where n is equal to two in the expression of $s_{z0}(z)$ in (55). It can be seen that the product $s_{z0}(z)\sigma_z(z)$ varies almost uniformly as a parabolic function in the entire region of the absorber. The selection of $s_{z0}(z)$, as expressed in (55), will typically make the value of $s_{z0}(z)$, especially near the outer computation boundary, much larger than one, so that the attenuation of evanescent waves is substantially accelerated.

It has been found that if the value of $s_{z0}(z)$ is too large, large numerical reflections can appear at high frequencies. The reason for this phenomenon, we think, is as follows. As $s_{z0}(z)$ increases in its value, the wavelength of the fields in the absorber decreases by a factor of $s_{z0}(z)$. We found that significant numerical reflection can be observed when the wavelength of the fields decreases to about two to three times the finite-difference space step. Therefore, the value of s_m needs to be bounded by the condition $\lambda/(1+s_m) > 2$ to 3 dh, where dh is the finite-difference space step and λ is the shortest wavelength of interest for the fields in the interior medium terminated by the absorber.

The value of σ_m can be determined from the theoretical reflection coefficient of the absorber. For example, when $n = 2$ in (55) and a perfect electric conductor is placed to terminate the absorber, the theoretical reflection coefficient $R_{\rm th}$ of the absorber for a normal incident propagating wave can be found as

$$R_{\rm th} = \exp\left[-\frac{2}{\epsilon c}\int_0^{\delta} s_{z0}(z)\sigma_z(z)\,dz\right] = \exp\left\{-\left[1+s_m\left(\frac{1}{3}+\frac{2}{\pi^2}\right)\right]\frac{\sigma_m\delta}{\epsilon c}\right\}. \quad (57)$$

From (57), the value of σ_m can be chosen as

$$\sigma_m = -\frac{\epsilon c/\delta}{1+s_m(1/3+2/\pi^2)}\ln R_{\rm th}. \quad (58)$$

VI. Numerical Tests

A. Performance of GPML for Waveguide Structures

Consider a rectangular waveguide filled with the free space. The wider side of the waveguide cross section is 40 mm. The FDTD space step dh is chosen to be 1 mm. The cutoff frequencies of TE10 and TE20 modes are at 3.75 and 7.5 GHz, respectively. A 16-cell-thick PML or GPML absorber to be tested with $R_{\rm th} = 10^{-4}$ is placed at the right end of the waveguide. The reflection coefficient of the absorber to be tested is measured at the interface of the free space and the absorber. The waveguide is excited by a sheet of current source located at one space step away from the tested absorber at the right and 75 space steps away from an "ideal" absorber at the left. The "ideal" absorber that simulates an infinite long waveguide is a 30-cell PML with $R_{\rm th} = 10^{-8}$. The "ideal" 30-cell PML provides near perfect absorption for propagating waves, while 75 space steps from the current source to the "ideal" absorber plus additional 30 space steps inside the absorber provide sufficient damping for the evanescent waves, probably except for a small frequency range near the cutoff frequency. The waveform of the current source is a 100-ps-wide Gaussian pulse modulated by a 15-GHz carrier. Since the medium inside the waveguide is lossless, the auxiliary variables are not necessary and only (44)–(47) are used. For GPML, the parameter s_m is set as five, so that when $\lambda/(1+s_m) = 3$, the frequency $f = 16.7$ GHz. The reflection coefficients of the 16-cell PML and GPML absorbers are shown in Fig. 3 for $\rm TE_{10}$ and $\rm TE_{20}$ modes. As can be seen from Fig. 3, PML can only absorb waves somewhat above the cutoff frequency, while the GPML cannot only absorb the propagating waves, but also adds a substantial damping to the evanescent waves.

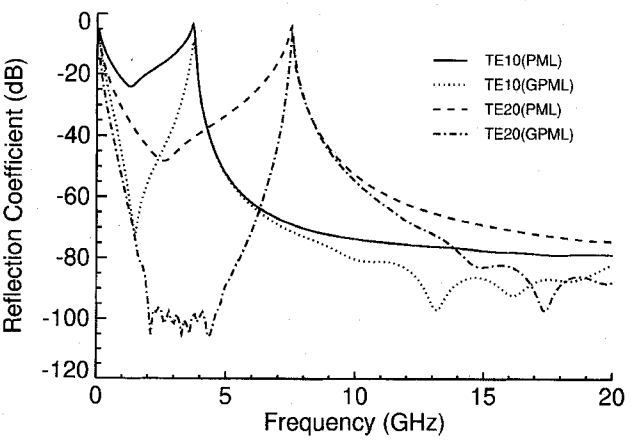

Fig. 3. Numerical reflection coefficients of $\rm TE_{10}$ and $\rm TE_{20}$ modes for 16-cell PML/GPML in a rectangular waveguide with the wider side of the waveguide cross section of 40 mm. The FDTD space step dh is 1 mm. The theoretical reflection coefficient of PML/GPML is set at $R_{\rm th} = 10^{-4}$, and $s_m = 5$ for GPML.

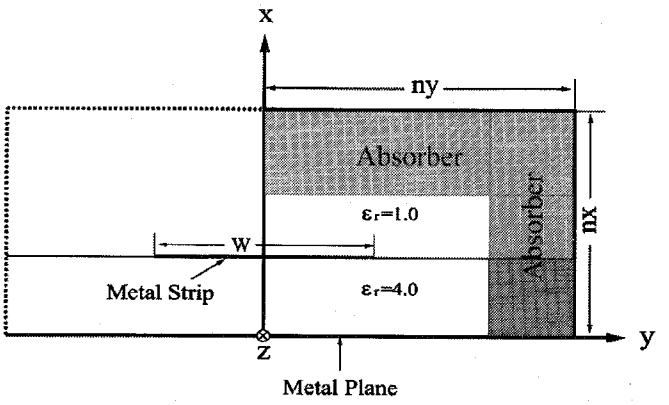

Fig. 4. Cross section of the computation domain for a microstrip line. The width of the metal strip is $W = 1000\,\mu$m. The thickness of the substrate $h = 500\,\mu$m. The space step $\Delta x = \Delta y = \Delta z = 125\,\mu$m. Due to the symmetry of the structure, half of the physical structure is computed.

In the above as well as following numerical tests, the conductivity profiles for PML and s_{x0}, s_{y0} and s_{z0} profiles for GPML are all chosen to be parabolic functions.

B. Performance of GPML for Microstrip Lines

To simulate a wave propagation along a microstrip line, PML/GPML is placed near the outer computation domain as shown in Fig. 4. Due to the symmetry of the structure, only half of the 3-D structure is computed, and the surface at the center of the metal strip is modeled as a magnetic wall. The dimensions in the transverse cross section of the computation domain are denoted as nx and ny as shown in Fig. 4. The relative dielectric constant of the substrate is four.

At the end surfaces perpendicular to the metal strip, where outgoing waves incident upon outer boundaries in near normal incident angles, PML/GPML works very well as expected. A 16-cell PML/GPML can easily make the reflection coefficient

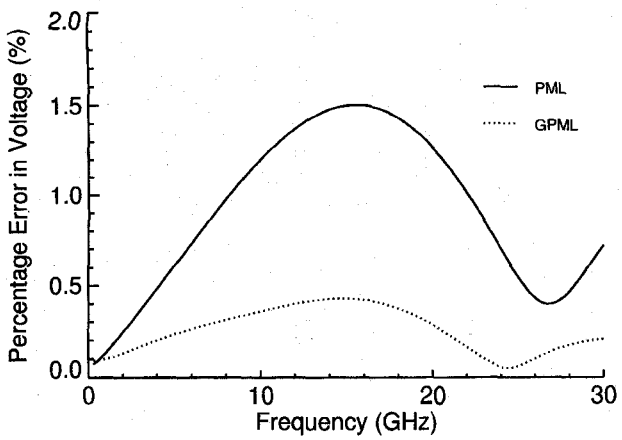

Fig. 5. Percentage errors in the computed voltage of the microstrip line of Fig. 4. The computation domain of the cross section is of 14 × 14 cells. The thickness of PML/GPML is eight cells. $R_{\text{th}} = 10^{-5}, s_m = 6$.

lower than −80 dB. On the top and the side surfaces of the computation domain, where fields are mostly evanescent in the direction normal to outer surfaces, GPML is found to be more effective than PML.

Fig. 5 shows the percentage errors in the computed voltage of the microstrip line for eight-cell PML and GPML absorbers placed on the top and the side surfaces of the computation domain, with $R_{\text{th}} = 10^{-5}$ and $s_m = 6$. The size of the computation domain in the transverse direction is chosen as $nx = ny = 14$ and $dh = 125\,\mu$m. The percentage errors in the voltage of the microstrip line is calculated with respect to the reference voltage obtained with a very large computation domain. The large computation domain is of the size $nx \times ny = 50 \times 50$, and is terminated by a 32-cell-thick GPML at each side, with $R_{\text{th}} = 10^{-10}$ and $s_m = 6$. The voltage of a microstrip line is calculated with the line integration of the electric field from reference plane to the metal strip. It can be seen from Fig. 5 that GPML results in smaller numerical error than PML.

C. Performance of GPML for Lossy Media

In order to evaluate the performance of the GPML for terminating lossy media, let us consider the configuration shown in Fig. 6. There are three lossy layers inside the computation domain. Suppose the electric conductivities of the lossy layers are $\sigma_0 = 0.1, 0.2, 0.3$ S/m and the magnetic conductivities σ_0^* are all equal to zero. The computation domain is of $100\,dh \times 50\,dh$, with $dh = 1.5$ cm. The computation results displayed are for the 2-D TE case. The excitation of the fields is through a point source at the mesh point (50, 25) by specifying

$$H_z(50,25) = \begin{cases} \frac{1}{320}(10 - 15\cos 2\pi t + 6\cos 4\pi t - \cos 6\pi t) \\ \qquad \text{for } t < 1 \text{ ns} \\ 0 \qquad \text{for } t > 1 \text{ ns.} \end{cases} \tag{59}$$

A reference solution is computed using a large domain of $400\,dh \times 400\,dh$. Denote $H_z(i,j)$ the field in the small domain with PML/GPML absorbers under test and $H_{zr}(i,j)$ the reference field computed with the large domain. The L^2 norm of the error in $H_z(i,j)$ is computed as

$$L^2 = \sum_{i=1}^{100}\sum_{j=1}^{50}[H_z(i,j) - H_{zr}(i,j)]^2. \tag{60}$$

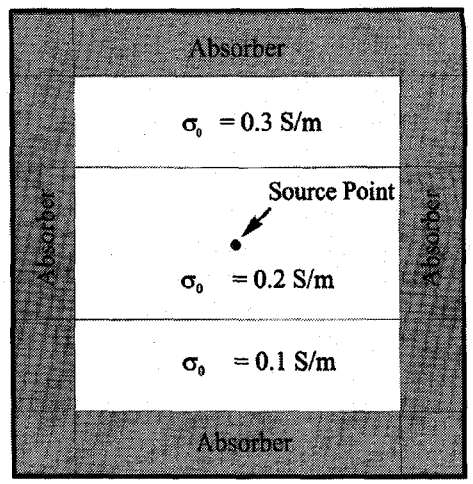

Fig. 6. Cross section of a layered lossy media terminated by PML/GPML absorber. The electric conductivities are $\sigma_0 = 0.1, 0.2, 0.3$ S/m, as shown in the figure, and magnetic conductivities are $\sigma_0^* = 0$ S/m. The size of the computation domain is 100 × 50 cells. A point source is located at the center of the computation domain.

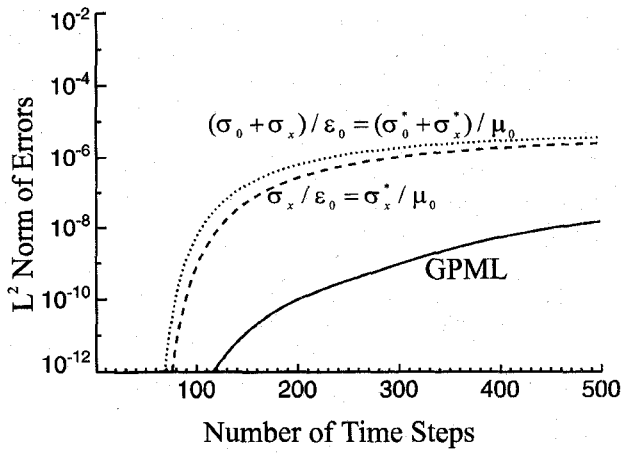

Fig. 7. The L^2 norm of the reflection error of PML/GPML versus number of time steps for the layered lossy media structure shown in Fig. 6.

Fig. 7 shows the results computed using a eight-cell GPML with $R_{\text{th}} = 10^{-4}, s_m = 6$ and using other two alternative eight-cell absorbers. Auxiliary variables representing the time integration of the corresponding field variables are used in implementing GPML. On the other hand, the implementations for the two alternative absorbers are the same as that for the original PML. In one alternative absorber, the σ_x and σ_x^* are simply chosen according to $\sigma_x/\epsilon_0 = \sigma_x^*/\mu_0$, while in the other alternative absorber, $(\sigma_0+\sigma_x)/\epsilon_0 = (\sigma_0^*+\sigma_x^*)/\mu_0$. The σ_x and σ_x^* of the two alternative absorbers are selected according to $R_{\text{th}} = 10^{-4}$ for terminating a lossless medium. As can be seen from Fig. 7, reflection errors of the two alternative absorbers, since they do not match the internal lossy media, are much larger than the reflection error of the GPML absorber.

VII. Conclusion

This paper presents the GPML technique that can be applied to absorb both propagating and evanescent waves in lossless and/or lossy medium. Numerical tests on waveguide structures, microstrip lines, and layered lossy media problems show that the generalized perfectly matched layer can lead to numerical solutions with very small numerical errors that can hardly be achieved by the original perfectly matched layer. Further extension of the generalized perfectly matched layer method to lossy dispersive media is straightforward by applying the existing techniques in dealing with dispersive media [14], [15]. Potential problems in absorbing evanescent waves in lossy media at low frequencies need to be studied further.

References

[1] J. P. Berenger, "A perfectly matched layer for the absorption of electromagnetic waves," *J. Comput. Physics*, vol. 114, Oct. 1994, pp. 185–200.

[2] R. Holland and J. W. Williams, "Total-field versus scattered-field finite-difference codes: A Comparative Assessment," *IEEE Trans. Nucl. Sci.*, vol. NS-30, no. 6, pp. 4583–4588, Dec 1983,

[3] D. S. Katz, E. T. Thiele, and A. Taflove, "Validation and extension to three dimensions of the berenger pml absorbing boundary condition for FD-TD meshes," *IEEE Microwave Guided Wave Lett.*, vol. 4, no. 8, pp. 268–270, Aug. 1994.

[4] Z. Wu and J. Fang, "Performance of the perfectly matched layer in modeling wave propagation in microwave and digital circuit interconnects," in *Proc. 11th Annu. Review of Progress in Applied Computational Electromagnetics*, Monterey, CA, Mar. 20–25, 1995, pp. 504–511.

[5] M. Gribbons, S. K. Lee, and A. C. Cangellaris, "Modification of Berenger's perfectly matched layer for the absorption of electromagnetic waves in layered media," in *Proc. 11th Annu. Review of Progress in Applied Computational Electromagnetics*, Monterey, CA, Mar. 20–25, 1995, pp. 498–503.

[6] Z. Wu and J. Fang, "Numerical implementation and performance of perfectly matched layer boundary condition for waveguide structures," *IEEE Trans. Microwave Theory Tech.*, vol. 43, no. 12, pp. 2676–2683, Dec. 1995.

[7] J. D. Moerloose and M. A. Stuchly, "Behavior of Berenger's ABC for evanescent waves," *IEEE Microwave Guided Wave Lett.*, vol. 5, no. 10, pp. 344–346, Aug. 1995.

[8] D. M. Kingsland, Z. S. Sacks, and J. F. Lee, "Perfectly matched anisotropic absorbers for finite element applications in electromagnetics," in *Proc. 11th Annu. Review of Progress in Applied Computational Electromagnetics*, Monterey, CA, Mar. 20–25, 1995, pp. 490–497.

[9] J. Fang and Z. Wu, "Generalized perfectly matched layer—An extension of berenger's perfectly matched layer boundary condition," *IEEE Microwave Guided Wave Lett.*, pp. 451–453, Dec. 1995.

[10] W. C. Chew and W. H. Weedon, "A 3D perfectly matched medium from modified Maxwell s equations with stretched coordinates," *Microwave Opt. Technol. Lett.*, vol. 7, no. 13, pp. 599–604, Sept. 1994.

[11] D. S. Katz, C. E. Reuter, E. T. Thiele, R. M. Joseph, and A. Taflove, "Extension of FD-TD Simulation Capabilities using the Berenger PML," in *1995 Dig. USNC/URSI Radio Science Meet.*, Newport Beach, CA, p. 334.

[12] S. D. Gedney and A. Roden, "Applying Berenger's perfectly matched layer (PML) boundary condition to non-orthogonal FDTD analyzes of planar microwave circuits," in *1995 Dig. USNC/URSI Radio Science Meet.*, Newport Beach, CA, p. 333.

[13] Z. Wu and J. Fang, "Experiments on the perfectly matched layer boundary condition in modeling wave propagation in waveguide components," in *1995 Dig. USNC/URSI Radio Science Meet.*, Newport Beach, CA, p. 336.

[14] K. S. Kunz and R. J. Luebbers, *The Finite-Difference Time-Domain Method for Electromagnetics*. Boca Raton, FL: CRC, 1993, ch. 8, pp. 123–162.

[15] A. Taflove, *Computational Electromagnetics, The Finite-Difference Time-Domain Method*. Dedham, MA: Artech House, 1995, ch. 9, pp. 227–280.

Jiayuan Fang (S'85–M'90) received the M.S. and Ph.D. degrees in electrical engineering from the University of California, Berkeley, in 1987 and 1989, respectively.

He was an Assistant Professor from 1990 to 1994, and an Associate Professor since 1995, Department of Electrical Engineering, State University of New York at Binghamton. His research interests are in applied electromagnetics, numerical methods, and electromagnetic modeling and simulation of electronic packaging.

Dr. Fang has been serving as an Associate Editor for IEEE Transactions on Components, Packaging, and Manufacturing Technology/Part B: Advanced Packaging since 1994. He received the National Science Foundation Research Initiation Award (RIA) in 1991 and Young Investigator Award (NYI) in 1993.

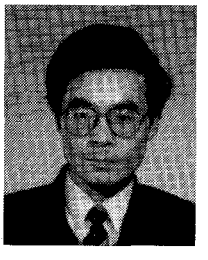

Zhonghua Wu (S'93) was born in Jiangsu Province, P. R. China, on April 22, 1966. He received the B.S. degree in geophysics from the University of Science and Technology of China in 1989, the M.S. degree in geophysics from the Institute of Geophysics, Chinese Academy of Science, in 1992, and the M.S. and Ph.D. degrees in electrical engineering from the State University of New York at Binghamton in 1995 and 1996, respectively. In his Ph.D. research, he worked on the development of high-performance perfectly matched layer and its application to waveguide structures and digital circuit interconnects.

Currently, he is working at LSI Logic Inc. as a Design Engineer. His areas of professional interest include numerical techniques in electromagnetics, transmission line theories, modeling and simulation of electronic packaging, on-chip and off-chip signal integrity analysis, VLSI design, fast circuit and field simulation tool development, and wireless communication.